

NAVAL POSTGRADUATE SCHOOL MONTEREY, CALIFORNIA



THESIS

THE MACH-ZEHNDER COUPLER

by

Joseph S. Gildersleeve

December, 1997

Thesis Advisors:

John P. Powers
D. Scott Davis

Approved for public release; distribution is unlimited.

DTIC QUALITY INSPECTED 3

19980414 041

REPORT DOCUMENTATION PAGE			Form Approved OMB No. 0704-0188	
Public reporting burden for this collection of information is estimated to average 1 hour per response, including the time for reviewing instruction, searching existing data sources, gathering and maintaining the data needed, and completing and reviewing the collection of information. Send comments regarding this burden estimate or any other aspect of this collection of information, including suggestions for reducing this burden, to Washington Headquarters Services, Directorate for Information Operations and Reports, 1215 Jefferson Davis Highway, Suite 1204, Arlington, VA 22202-4302, and to the Office of Management and Budget, Paperwork Reduction Project (0704-0188) Washington DC 20503.				
1. AGENCY USE ONLY (Leave blank)	2. REPORT DATE December 1997	3. REPORT TYPE AND DATES COVERED Master's Thesis		
4. TITLE AND SUBTITLE THE MACH-ZEHNDER COUPLER		5. FUNDING NUMBERS		
6. AUTHOR(S) Joseph S. Gildersleeve				
7. PERFORMING ORGANIZATION NAME(S) AND ADDRESS(ES) Naval Postgraduate School Monterey CA 93943-5000		8. PERFORMING ORGANIZATION REPORT NUMBER		
9. SPONSORING/MONITORING AGENCY NAME(S) AND ADDRESS(ES)		10. SPONSORING/MONITORING AGENCY REPORT NUMBER		
11. SUPPLEMENTARY NOTES The views expressed in this thesis are those of the author and do not reflect the official policy or position of the Department of Defense or the U.S. Government.				
12a. DISTRIBUTION/AVAILABILITY STATEMENT Approved for public release; distribution is unlimited.			12b. DISTRIBUTION CODE	
13. ABSTRACT (maximum 200 words) This thesis is the second in a series which investigates the possibility of creating a code-shift-keying (CSK) optical receiver using single-mode 2x2 couplers and fiber optical delay lines to construct Mach-Zehnder couplers which comprise the main building block of the CSK receiver. There were two main goals of this thesis research. The first was to investigate design and construction modifications which would lower the system loss of a previously designed Mach-Zehnder coupler. As a result of this research, the system loss was reduced from 10.5 dB to 3.3 dB by changing the design to eliminate an unnecessary stage and by replacing several mechanical connections with fusion splices. The second goal was to find a method to measure the inherent phase shift of a 2x2 fiber optical coupler. Two separate methods were developed and implemented, and a third previously developed method was used to verify the results. All three methods provided experimental values between 145° and 149°. This thesis develops the theory that explains the discrepancy between the measured values and the ideal value of 180° for the inherent phase shift				
14. SUBJECT TERMS Fiber Optic Receiver, Mach-Zehnder coupler, Interferometry			15. NUMBER OF PAGES 54	
			16. PRICE CODE	
17. SECURITY CLASSIFICATION OF REPORT Unclassified	18. SECURITY CLASSIFICATION OF THIS PAGE Unclassified	19. SECURITY CLASSIFICATION OF ABSTRACT Unclassified	20. LIMITATION OF ABSTRACT UL	

Approved for public release; distribution is unlimited.

THE MACH-ZEHNDER COUPLER

Joseph S. Gildersleeve
Lieutenant Commander, United States Navy
B.S., The Pennsylvania State University, 1984

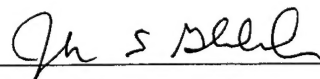
Submitted in partial fulfillment
of the requirements for the degrees of

MASTER OF SCIENCE IN ELECTRICAL ENGINEERING AND MASTER OF SCIENCE IN APPLIED PHYSICS

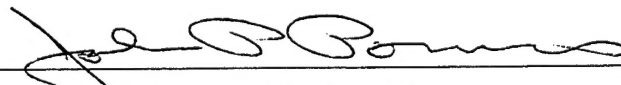
from the

NAVAL POSTGRADUATE SCHOOL
December 1997

Author:

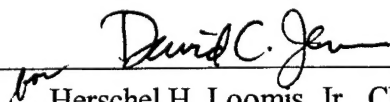

Joseph S. Gildersleeve

Approved by:


John P. Powers, Thesis Advisor



D. Scott Davis, Thesis Advisor



Herschel H. Loomis, Jr., Chairman

Department of Electrical and Computer Engineering



William B. Maier II, Chairman

Department of Physics

ABSTRACT

This thesis is the second in a series which investigates the possibility of creating a code-shift-keying (CSK) optical receiver using single-mode 2x2 couplers and fiber optical delay lines to construct Mach-Zehnder couplers which comprise the main building block of the CSK receiver. There were two main goals of this thesis research. The first was to investigate design and construction modifications which would lower the system loss of a previously designed Mach-Zehnder coupler. As a result of this research, the system loss was reduced from 10.5 dB to 3.3 dB by changing the design to eliminate an unnecessary stage and by replacing several mechanical connections with fusion splices. The second goal was to find a method to measure the inherent phase shift of a 2x2 fiber optical coupler. Two separate methods were developed and implemented, and a third previously developed method was used to verify the results. All three methods provided experimental values between 145° and 149° . This thesis develops the theory that explains the discrepancy between the measured values and the ideal value of 180° for the inherent phase shift.

TABLE OF CONTENTS

I. INTRODUCTION	1
II. THE MACH-ZEHNDER COUPLER	5
A. BACKGROUND	5
B. SIGNAL ANALYSIS.....	7
1. System Overview.....	8
2. The 2x2 Coupler.....	8
3. Delay Line.....	9
4. System Analysis.....	10
5. Time Domain Analysis.....	11
C. SYSTEM WITH IDEAL COUPLERS	13
1. Ideal 2x2 Coupler	13
2. Ideal Delay Line	13
3. Ideal System Analysis	13
D. MULTI-STAGE RECEIVER	14
III. COUPLER PHASE SHIFT ANALYSIS	17
A. BACKGROUND	17
B. APPLICATION OF DC VOLTAGE TO PZT TO CONTROL OPTICAL PATH DIFFERENCE	17
1. Derivation	17
2. Response of PZT device	19
3. Experimental Results	22
C. CALCULATION OF INHERENT PHASE SHIFT BY MEANS OF COUPLER EXCESS LOSS MEASUREMENT	22
1. Derivation	22
2. Experimental Results	25
D. APPLICATION OF AC VOLTAGE TO PZT TO DETERMINE PHASE SHIFT	25
1. Derivation	25
2. Experimental Results	28

E. CONCLUSIONS.....	29
IV. SYSTEM LOSS CONSIDERATIONS	33
A. PREVIOUS DESIGN	33
1. System Design.....	33
2. System Loss	34
B. CURRENT DESIGN	34
C. LOSS IMPROVEMENT ANALYSIS.....	35
1. Comparison of Previous and Current System Loss.....	35
2. Analysis of Improvement	36
3. Multi-stage Receiver.....	38
V. CONCLUSIONS.....	39
LIST OF REFERENCES	43
INITIAL DISTRIBUTION LIST	45

I. INTRODUCTION

Fiber optics have become increasingly important in modern communication systems. Fiber optic transmission systems have extremely high data rate capabilities and use small diameter, light weight cables providing superior communication security and near immunity to electromagnetic inference. Because of these outstanding characteristics, the U. S. Navy has implemented fiber optics in its newest ship designs.

Previous work conducted at the Naval Postgraduate School investigated the feasibility of designing and constructing a new type of optical signal demultiplexer, based on the concept of code-shift-keying [Ref. 1]. This thesis is the second in this area and concentrates on the analysis and improvement of a single building block of a multi-channel code shift keying receiver. This building block is the fiber optical counterpart of the classical Mach-Zehnder interferometer, with fiber couplers employed as beam splitters.

The two-stage Mach-Zehnder coupler (MZC) is shown in Figure 1.1.

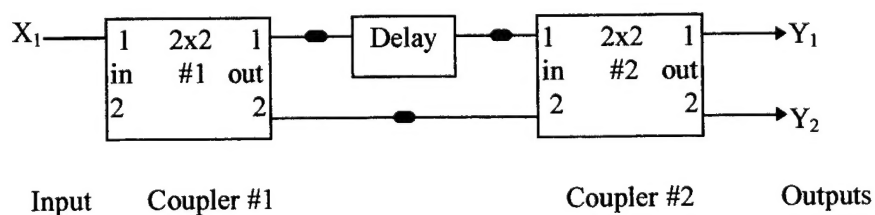


Figure 1.1. Two-stage Mach-Zehnder Coupler

The input, X_1 , consists of laser light that has been amplitude modulated by a digital data waveform. The MZC consists of two 2x2 single mode couplers and a delay line, the length of which is set to generate a delay equal to an integer number of bit periods of the

data waveform. The delay line and couplers are connected via either ST connectors or fusion splices. The 2x2 couplers divide the power of the input signals equally between their output channels. The 2x2 couplers also impart a phase shift in the optical carrier signal between the two output channels. The receiver takes advantage of this inherent phase shift to generate output power waveforms which are the sum and difference of sequential bits in the datastream.

If Mach-Zehnder couplers with various delay times are combined, a code shift keying (CSK) demultiplexer could be constructed. Figure 1.2 shows a CSK receiver which can discriminate between four CSK signals. The design could be repeated for n stages such that 2^n different CSK signals could be discriminated. In Chapter II, we develop the frequency and time domain signal analysis of the two-stage MZC and show that this two-stage design will function in a multi-stage receiver.

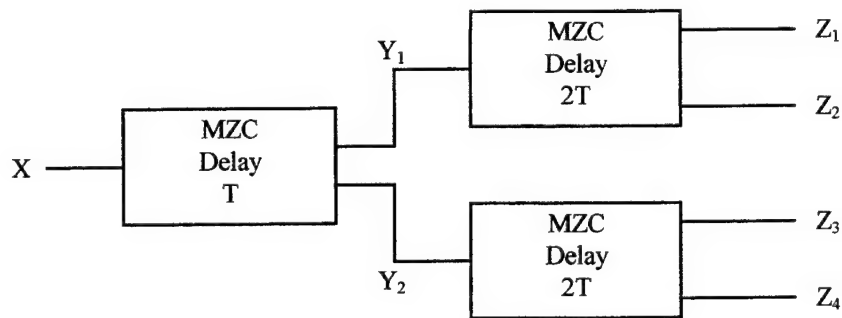


Figure 1.2. Multi-stage CSK Receiver

Because the MZC uses the inherent phase shift of the 2x2 coupler to generate the desired outputs, one of the major goals of this work was to find a method whereby the inherent phase shift of a 2x2 coupler can be measured. We were able to develop and to implement two separate techniques and to use a third technique described by Hereth and

Schliep [Ref. 2] to verify our results. Chapter III explains the three techniques and gives the results obtained using each method.

The other major goal of this work was to reduce the system loss from the previous design used by Heinbaugh [Ref. 1]. The previous design had a substantial loss for each MZC, making the loss for a a multi-stage CSK receiver very high. Chapter IV describes the design changes and construction techniques used to achieve the desired reduction in system loss.

Chapter V summarizes the conclusions from the design, construction and testing of the two-stage MZC. Analysis of the phase measurement techniques and loss improvement efforts are provided along with discussion of potential follow-on work.

II. THE MACH-ZEHNDER COUPLER

A. BACKGROUND

The basic building block of the code shift keying receiver is the Mach-Zehnder coupler (MZC). The MZC is a fiber optic version of the classic Mach-Zehnder interferometer, shown in Figure 2.1. The Mach-Zehnder interferometer consists of two beamsplitters and two totally reflective mirrors. The difference between the optical path lengths can be controlled by slightly tilting one of the beamsplitters or one of the mirrors, or by changing the refractive index of the medium in one of the arms. This difference in optical path length causes interference between the two waves when they are recombined at the second beamsplitter. The detector measures the resultant sum of the two waves [Ref. 3]. The Mach-Zehnder interferometer can also be constructed to provide a variable phase delay [Ref. 4].

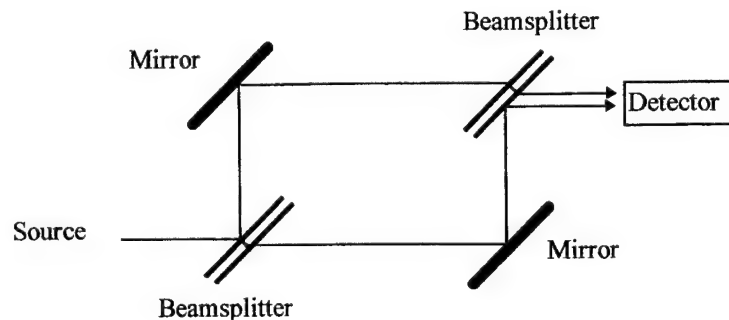


Figure 2.1. The Mach-Zehnder Interferometer

The Mach-Zehnder coupler is a fiber optic version of the Mach-Zehnder interferometer in which the beamsplitters are replaced by fiber optic single mode 2x2 couplers and a section of fiber is inserted as a delay line. Previous MZC designs studied at

the Naval Postgraduate School involved a third 2x2 coupler in the Y_2 output serving as a 90 degree phase shifter. In order to balance the 3 dB loss inherent in the third coupler, a corresponding 3 dB attenuator was inserted in the fiber parallel to this stage in the Y_1 output. Since the third stage was inserted to impart a 90 degree phase shift in the optical carrier signal and the optical signals are detected with PIN receivers, the exact phase of the optical carrier is not important since only the power in the signal is used for demultiplexing. Therefore, we have determined that the third coupler stage is unnecessary, and it is omitted in this design. The signal analysis of the two-stage Mach-Zehnder coupler and its application to a multi-stage receiver are developed in this chapter.

In order to follow the mathematical development of the Mach-Zehnder coupler, it is beneficial to review phasor notation. The signals involved in the system represent the electric field in the fiber optic components. We can express the electric field as a function of time and position as

$$E(z, t) = E_0 \cos(\omega t - kz + \varphi) = \text{Re} \left\{ E_0 e^{j\varphi} e^{j(\omega t - kz)} \right\}, \quad (2.1)$$

where $E(z, t)$ is the electric field at time t and position z , E_0 is the magnitude of the field, k is the wave spatial frequency ($2\pi/\lambda$) and φ is the initial phase of the signal. The electric field is equivalently expressed in phasor notation using the relationship

$$\tilde{E} = E_0 e^{j\varphi} \quad (2.2)$$

where the tilde over the E represents a phasor term corresponding to amplitude E_0 and phase φ and the sinusoidal time dependence is implied. Converting from phasor representation back to time domain representation involves multiplying the phasor by

$e^{j(\omega t - kz)}$ and taking the real part. Each component through which the signal passes affects its amplitude and phase. These effects can be represented by a phasor transfer function for each component. The transfer function of the component is multiplied by the input signal phasor to yield the phasor representation of the output. For a component with more than one input and one output, each input signal is related to each output signal by a separate phasor term in a matrix transfer function. For the system shown in Figure 2.2, the output is related to the input by the transfer function of the system in equation form by $\bar{Y} = \bar{A} \bar{X}$, where each term represents a matrix of phasor quantities.

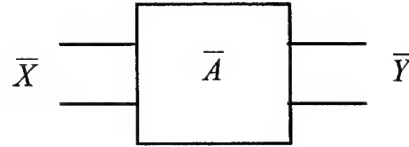


Figure 2.2. Phasor Component Representation

In describing the signal analysis of the Mach-Zehnder coupler, lower case letters will represent functions of time, upper case letters with a tilde will represent phasor quantities, and upper case letters with a bar will represent matrices comprised of phasors.

B. SIGNAL ANALYSIS

In this section we conduct mathematical analysis of the components of and signals in the Mach-Zehnder coupler.

1. System Overview

The two-stage Mach-Zehnder coupler is shown in Figure 2.3. The 2x2 couplers, designated by A and B , are single mode devices. The dark vertical lines represent connections between fibers. These connections may be fusion splices or a pair of ST

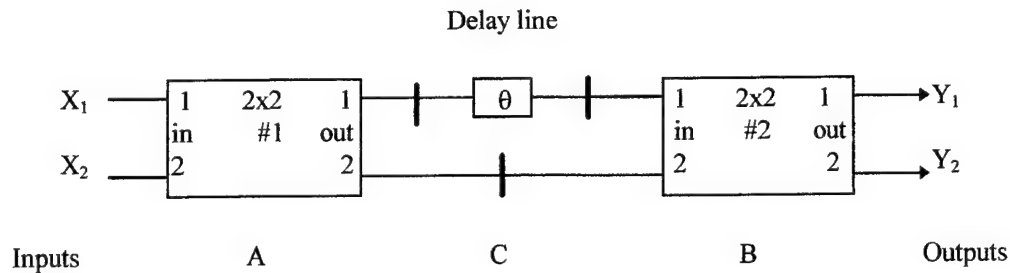


Figure 2.3. The Mach-Zehnder Coupler

connectors joined via an adapter. The delay line may be either a fixed-length section of single mode fiber or a section of fiber attached to a cylindrical piezoelectric transducer (PZT), which allows the user to vary the length of the fiber by controlling the voltage applied to the PZT. The coupler shown in Figure 2.3 can be represented by the matrix equation

$$\bar{Y} = \bar{B} \bar{C} \bar{A} \bar{X}, \quad (2.3)$$

where \bar{Y} represents the outputs, \bar{A} and \bar{B} represent the scattering matrices for the first and second couplers, respectively, \bar{C} represents the transfer function of the delay line section and its connections and \bar{X} represents the inputs into the first coupler.

2. The 2x2 Coupler

In general, the scattering matrix for a four terminal 2x2 coupler is a 4 by 4 matrix,

$$\bar{A} = \begin{bmatrix} \tilde{A}_{11} & \tilde{A}_{12} & \tilde{A}_{13} & \tilde{A}_{14} \\ \tilde{A}_{21} & \tilde{A}_{22} & \tilde{A}_{23} & \tilde{A}_{24} \\ \tilde{A}_{31} & \tilde{A}_{32} & \tilde{A}_{33} & \tilde{A}_{34} \\ \tilde{A}_{41} & \tilde{A}_{42} & \tilde{A}_{43} & \tilde{A}_{44} \end{bmatrix} \quad (2.4)$$

where

$$\tilde{A}_{mn} = A_{mn} e^{j\alpha_{mn}}, \quad (2.5)$$

such that each matrix element is a phasor quantity with amplitude and phase. Actual 2x2 couplers have very low reflectance, on the order of -30 dB or lower. Therefore, we can approximate the reflectance coefficients by zero, yielding a sparse matrix with simpler structure. We can then represent the scattering matrix for the first 2x2 coupler as

$$\bar{A} = \begin{bmatrix} \tilde{A}_{11} & \tilde{A}_{12} \\ \tilde{A}_{21} & \tilde{A}_{22} \end{bmatrix} = \begin{bmatrix} A_{11}e^{j\alpha_{11}} & A_{12}e^{j\alpha_{12}} \\ A_{21}e^{j\alpha_{21}} & A_{22}e^{j\alpha_{22}} \end{bmatrix}, \quad (2.6)$$

where the indices have been reassigned for convenience. Thus the term A_{12} corresponds to the magnitude of the scattering matrix coefficient relating the signal at output 1 to the signal at input 2. In the Mach-Zehnder coupler, the second 2x2 coupler has a similar scattering matrix, where the A 's would be replaced by B 's, and the α 's would be replaced by β 's.

3. Delay Line

The matrix representation of the connections between the couplers and delay line is

$$\bar{C} = \begin{bmatrix} C_{11}e^{-j\theta} & 0 \\ 0 & C_{22} \end{bmatrix} \quad (2.7)$$

where C_{11} and C_{22} represent the magnitudes of the amplitude coupling of the connections and are ≤ 1.0 , while θ represents the phase shift due to the difference in optical path lengths of the two fibers.

4. System Analysis

Substituting Equations 2.6 and 2.7 into Equation 2.3, expanding and simplifying yields

$$\bar{Y} = \begin{bmatrix} \tilde{A}_{11} \tilde{B}_{11} C_{11} e^{-j\theta} + \tilde{A}_{21} \tilde{B}_{12} C_{22} \\ \tilde{A}_{11} \tilde{B}_{21} C_{11} e^{-j\theta} + \tilde{A}_{21} \tilde{B}_{22} C_{22} \end{bmatrix} \bar{X}. \quad (2.8)$$

Equation 2.8 relates the outputs, \bar{Y} , to the inputs \bar{X} . In the system under consideration, \tilde{X}_2 will always be zero. Thus, the outputs are given by

$$\tilde{Y}_1 = \left(A_{11} B_{11} C_{11} e^{j(\alpha_{11} + \beta_{11} - \theta)} + A_{21} B_{12} C_{22} e^{j(\alpha_{21} + \beta_{12})} \right) \tilde{X}_1 \quad (2.9)$$

$$\tilde{Y}_2 = \left(A_{11} B_{21} C_{11} e^{j(\alpha_{11} + \beta_{21} - \theta)} + A_{21} B_{22} C_{22} e^{j(\alpha_{21} + \beta_{22})} \right) \tilde{X}_1. \quad (2.10)$$

Factoring the phase terms in Equations 2.9 and 2.10 yields

$$\tilde{Y}_1 = \left(A_{11} B_{11} C_{11} e^{-j\theta} + A_{21} B_{12} C_{22} e^{j(\alpha_{21} - \alpha_{11} + \beta_{12} - \beta_{11})} \right) e^{j(\alpha_{11} + \beta_{11})} \tilde{X}_1 \quad (2.11)$$

$$\tilde{Y}_2 = \left(A_{11} B_{21} C_{11} e^{-j\theta} + A_{21} B_{22} C_{22} e^{j(\alpha_{21} - \alpha_{11} + \beta_{22} - \beta_{21})} \right) e^{j(\alpha_{11} + \beta_{21})} \tilde{X}_1. \quad (2.12)$$

The outputs, \tilde{Y}_1 and \tilde{Y}_2 are sent to PIN receivers where the power in these outputs, represented by $|Y_1|^2$ and $|Y_2|^2$, is detected. Therefore, the absolute phase of the carrier signal is not important and the common phase terms may be neglected. Dropping the common phase terms, Equations 2.11 and 2.12 can be written as

$$\tilde{Y}_1 = \left(A_{11} B_{11} C_{11} e^{-j\theta} + A_{21} B_{12} C_{22} e^{j(\alpha_{21} - \alpha_{11} + \beta_{12} - \beta_{11})} \right) \tilde{X}_1 \quad (2.13)$$

$$\tilde{Y}_2 = \left(A_{11}B_{21}C_{11}e^{-j\theta} + A_{21}B_{22}C_{22}e^{j(\alpha_{21}-\alpha_{11}+\beta_{22}-\beta_{21})} \right) \tilde{X}_1. \quad (2.14)$$

Equations 2.13 and 2.14 will be used for derivations involving further signal analysis of the system and will be used in Chapter III to determine the inherent phase shift of a 2x2 coupler.

5. Time Domain Analysis

In order to develop expressions for the time domain output signals, $y_1(t)$ and $y_2(t)$, we make use of the Fourier shift theorem

$$y(t - t_0) \Leftrightarrow Y(\nu) \exp(-j2\pi\nu t_0). \quad (2.15)$$

Taking the inverse Fourier transform of Equations 2.13 and 2.14 yields

$$y_1(t) = A_{11}B_{11}C_{11} \cdot x_1\left(t - \frac{\theta}{2\pi\nu}\right) + A_{21}B_{12}C_{22} \cdot x_1\left(t + \frac{\alpha_{21} - \alpha_{11} + \beta_{12} - \beta_{11}}{2\pi\nu}\right) \quad (2.16)$$

$$y_2(t) = A_{11}B_{21}C_{11} \cdot x_1\left(t - \frac{\theta}{2\pi\nu}\right) + A_{21}B_{22}C_{22} \cdot x_1\left(t + \frac{\alpha_{21} - \alpha_{11} + \beta_{22} - \beta_{21}}{2\pi\nu}\right). \quad (2.17)$$

The input signal, $x_1(t)$, is given by

$$x_1(t) = d(t) \cos(2\pi\nu t), \quad (2.18)$$

where $\cos(2\pi\nu t)$ represents the optical carrier signal and $d(t)$ represents the modulating data signal. Substituting Equation 2.18 into Equations 2.16 and 2.17 yields

$$\begin{aligned} y_1(t) = & A_{11}B_{11}C_{11} \cdot d\left(t - \frac{\theta}{2\pi\nu}\right) \cos(2\pi\nu t - \theta) \\ & + A_{21}B_{12}C_{22} \cdot d\left(t + \frac{\alpha_{21} - \alpha_{11} + \beta_{12} - \beta_{11}}{2\pi\nu}\right) \cos(2\pi\nu t + (\alpha_{21} - \alpha_{11} + \beta_{12} - \beta_{11})) \end{aligned} \quad (2.19)$$

$$\begin{aligned}
y_2(t) = & A_{11}B_{21}C_{11} \cdot d\left(t - \frac{\theta}{2\pi\nu}\right) \cos(2\pi\nu t - \theta) \\
& + A_{21}B_{22}C_{22} \cdot d\left(t + \frac{\alpha_{21} - \alpha_{11} + \beta_{22} - \beta_{11}}{2\pi\nu}\right) \cos\left(2\pi\nu t + (\alpha_{21} - \alpha_{11} + \beta_{22} - \beta_{11})\right).
\end{aligned} \tag{2.20}$$

Equations 2.19 and 2.20 give the exact form of the output signals. It is instructive to consider the relative magnitude of the time delays imposed by the θ , α and β terms. For real couplers, the α and β terms correspond to phase shifts on the order of $\pi/2$ radians. With a wavelength of 1300 nm, the optical carrier frequency, ν , is about 2.3×10^{14} Hz. Thus, the magnitude of the time delay corresponding to the α and β terms is on the order of 10^{-15} seconds. Using a bit rate of 100 Mbps, or a bit period of 1×10^{-8} seconds, this time delay would correspond to a negligible fraction of a bit period. As stated earlier, the θ term represents the phase delay corresponding to the exact difference in optical path length of the two fibers connecting the two couplers. We can construct the circuit such that the difference in optical path length corresponds to one bit period. For the bit period of 1×10^{-8} seconds and a typical fiber core refractive index of 1.45, the length of fiber required to implement a one period delay is given by

$$L = \frac{Tc}{n} = \frac{(1 \cdot 10^{-8})(3 \cdot 10^8)}{1.45} = 2.07 \text{ meters}. \tag{2.21}$$

Since θ is contained only in the first terms of Equations 2.19 and 2.20, the delay line fiber length must only be accurate to within a fraction of a bit period, not within a fraction of a wavelength of the optical carrier. Deleting the time delay corresponding to the phase shift due to the α and β terms as discussed above and setting

$$\theta = 2\pi\nu T, \tag{2.22}$$

Equations 2.19 and 2.20 can be expressed as

$$y_1(t) = A_{11}B_{11}C_{11} \cdot d(t-T) \cos(2\pi\nu(t-T)) \\ + A_{21}B_{12}C_{22} \cdot d(t) \cos(2\pi\nu t + (\alpha_{21} - \alpha_{11} + \beta_{12} - \beta_{11})) \quad (2.23)$$

$$y_2(t) = A_{11}B_{21}C_{11} \cdot d(t-T) \cos(2\pi\nu(t-T)) \\ + A_{21}B_{22}C_{22} \cdot d(t) \cos(2\pi\nu t + (\alpha_{21} - \alpha_{11} + \beta_{22} - \beta_{21})). \quad (2.24)$$

C. SYSTEM WITH IDEAL COUPLERS

1. Ideal 2x2 Coupler

For an ideal 2x2 coupler, all scattering matrix coefficients have a magnitude of $(0.5)^{1/2}$, so that the input power is equally split between the two output fibers. Solution of the Maxwell equations inside the ideal coupler require that the scattering matrix coefficients have phases such that [Ref. 5]

$$\bar{A} = \bar{B} = \begin{bmatrix} \frac{1}{\sqrt{2}} e^{j0} & \frac{1}{\sqrt{2}} e^{j\pi/2} \\ \frac{1}{\sqrt{2}} e^{j\pi/2} & \frac{1}{\sqrt{2}} e^{j0} \end{bmatrix}. \quad (2.25)$$

2. Ideal Delay Line

If the delay line connections have no loss, then

$$C_{11} = C_{22} = 1, \quad (2.26)$$

3. Ideal System Analysis

Substitution of Equations 2.25 and 2.26 into 2.9 and 2.10 yields

$$\tilde{Y}_1 = 0.5(e^{-j\theta} - 1) \tilde{X}_1 \quad (2.27)$$

$$\tilde{Y}_2 = 0.5(e^{-j\theta} e^{j\pi/2} + e^{j\pi/2}) \tilde{X}_1. \quad (2.28)$$

Taking the inverse Fourier transform of Equations 2.27 and 2.28 yields

$$y_1(t) = 0.5 \left[x_1 \left(t - \frac{\theta}{2\pi\nu} \right) - x_1(t) \right] \quad (2.29)$$

$$y_2(t) = 0.5 \left[x_1 \left(t - \frac{\theta}{2\pi\nu} + \frac{1}{4\nu} \right) + x_1 \left(t + \frac{1}{4\nu} \right) \right]. \quad (2.30)$$

The terms in the expression for $y_2(t)$ have a time shift of $(0.25/\nu)$, corresponding to one-fourth of the period of the optical carrier signal, or approximately 10^{-15} seconds.

Compared to the one bit period inserted time delay (10^{-8} seconds), this delay is negligible.

Deleting this minor delay term and using Equation 2.22, Equations 2.29 and 2.30 can be expressed as

$$y_1(t) = 0.5 [x_1(t - T) - x_1(t)] \quad (2.31)$$

$$y_2(t) = 0.5 [x_1(t - T) + x_1(t)]. \quad (2.32)$$

From Equations 2.31 and 2.32, it is apparent that the top output from the Mach-Zehnder coupler, $y_1(t)$, is the difference of the previous bit and the current bit. The bottom output of the Mach-Zehnder coupler, $y_2(t)$, is the sum of the previous bit and the current bit.

D. MULTI-STAGE RECEIVER

Using the concepts derived in this chapter, we can construct a multi-stage receiver from the basic Mach-Zehnder coupler. Figure 2.4 shows a block diagram of a two-stage receiver, where the first stage is a MZC with a delay of one bit period, T . The second stage is made of two MZCs each with delay of two bit periods, $2T$. In Figure 2.4, X is the input to the MZC with delay T , Y_1 and Y_2 are the outputs from the first stage and

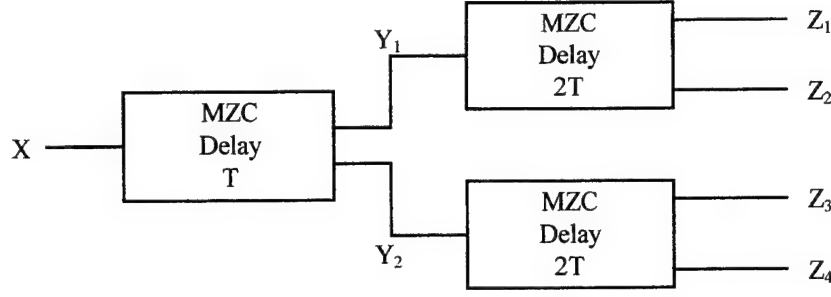


Figure 2.4. Multi-stage Receiver

Z_1 through Z_4 are the final outputs. By analogy with Equations 2.31 and 2.32, the intermediate outputs, Y_1 and Y_2 are given by

$$y_1(t) = 0.5[x(t-T) - x(t)] \quad (2.33)$$

$$y_2(t) = 0.5[x(t-T) + x(t)]. \quad (2.34)$$

For the MZCs with the $2T$ delay, similar equations exist for the outputs Z_1 through Z_4 , where T is replaced by $2T$. The outputs are given by

$$z_1(t) = 0.5[y_1(t-2T) - y_1(t)] \quad (2.35)$$

$$z_2(t) = 0.5[y_1(t-2T) + y_1(t)] \quad (2.36)$$

$$z_3(t) = 0.5[y_2(t-2T) - y_2(t)] \quad (2.37)$$

$$z_4(t) = 0.5[y_2(t-2T) + y_2(t)]. \quad (2.38)$$

Substitution of Equations 2.33 and 2.34 into 2.35 through 2.38 yields

$$z_1(t) = 0.25[x(t-3T) - x(t-2T) - x(t-T) + x(t)] \quad (2.39)$$

$$z_2(t) = 0.25[x(t-3T) - x(t-2T) + x(t-T) - x(t)] \quad (2.40)$$

$$z_3(t) = 0.25[x(t-3T) + x(t-2T) - x(t-T) - x(t)] \quad (2.41)$$

$$z_4(t) = 0.25[x(t-3T) + x(t-2T) + x(t-T) + x(t)]. \quad (2.42)$$

The four outputs all have the same amplitude, and each represents a different combination of the present data bit, $x(t)$, and the previous three bits, $x(t-T)$, $x(t-2T)$ and $x(t-3T)$. When the relative signs of the four data bits involved in the four outputs are compared, the four codes obtained have the bit pattern shown in Table 2.1. When the bit patterns in Table 2.1 are inspected, it is evident that the cross-correlation of the four codes are all zero. The four outputs provide four orthogonal Walsh-Hadamard sequence codes, which leads to the minimum bit error rate [Ref. 6]. Thus, we have shown in this section that the two-stage MZC may be used to construct the multi-stage receiver shown in Figure 2.4.

	$X(t-3T)$	$X(t-2T)$	$X(t-T)$	$X(t)$
Z_1	1	-1	-1	1
Z_2	1	-1	1	-1
Z_3	1	1	-1	-1
Z_4	1	1	1	1

Table 2.1. Temporal Structure of Bit Pattern of Four Output Codes

In the next chapter, we investigate three separate methods used to measure the inherent phase shift of the 2x2 couplers used in the Mach-Zehnder coupler.

III. COUPLER PHASE SHIFT ANALYSIS

A. BACKGROUND

As shown in the previous chapter, the inherent phase shift of a 2x2 coupler is used to provide the sum and difference outputs from the Mach-Zehnder Coupler. In this chapter we develop three separate methods for measuring the inherent phase shift of a 2x2 coupler, defined as $(\beta_{21} - \beta_{22} + \beta_{12} - \beta_{11})$.

B. APPLICATION OF DC VOLTAGE TO PZT TO CONTROL OPTICAL PATH DIFFERENCE

1. Derivation

The first method for measuring the coupler phase shift uses optical fiber wrapped around a cylindrical PZT as the “delay line”, as shown in Figure 3.1. A DC voltage is applied between the inner and outer surfaces of the PZT. The input is provided by a laser diode run at constant power. Using a variable voltage source connected to the PZT cylinder allows fine control of the total optical path length of the fiber connecting output 1 of the first coupler to input 1 of the second coupler and, thus, the optical path difference between the fibers connecting ports one and two of the couplers. The optical path

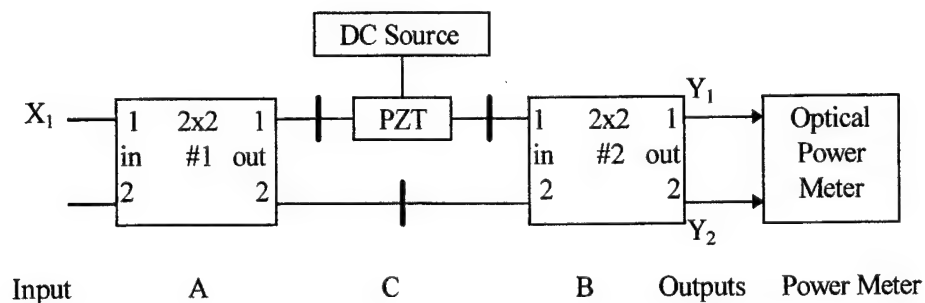


Figure 3.1. System for DC Control Phase Measurement

difference was represented by θ in the development in Chapter II. Since the outputs, Y_1 and Y_2 , are detected by PIN devices, only the power in the signal is important. From Equations 2.13 and 2.14, it can be shown that the power in the outputs, for general θ , is given by

$$|Y_1|^2 = \left[(A_{21}B_{12}C_{22})^2 + (A_{11}B_{11}C_{11})^2 + 2A_{11}A_{21}B_{11}B_{12}C_{11}C_{22} \cdot \cos(\theta - \beta_{11} + \beta_{12} + \alpha_{21} - \alpha_{11}) \right] \cdot |X_1|^2 \quad (3.1)$$

$$|Y_2|^2 = \left[(A_{21}B_{22}C_{22})^2 + (A_{11}B_{21}C_{11})^2 + 2A_{11}A_{21}B_{21}B_{22}C_{11}C_{22} \cdot \cos(\theta - \beta_{21} + \beta_{22} + \alpha_{21} - \alpha_{11}) \right] \cdot |X_1|^2 \quad (3.2)$$

If the voltage applied to the PZT is varied such that

$$\theta = \beta_{11} - \beta_{12} - \alpha_{21} + \alpha_{11} + \pi, \quad (3.3)$$

then Equations 3.1 and 3.2 can be reduced to

$$|Y_1|_{\min}^2 = (A_{21}B_{12}C_{22} - A_{11}B_{11}C_{11})^2 \cdot |X_1|^2 \quad (3.4)$$

$$|Y_2|_{\max}^2 = \left[(A_{21}B_{22}C_{22})^2 + (A_{11}B_{21}C_{11})^2 - 2A_{11}A_{21}B_{21}B_{22}C_{11}C_{22} \cdot \cos(\beta_{21} - \beta_{22} + \beta_{12} - \beta_{11}) \right] \cdot |X_1|^2 \quad (3.5)$$

If the DC voltage applied to the PZT is adjusted such that

$$\theta = \beta_{11} - \beta_{12} - \alpha_{21} + \alpha_{11}, \quad (3.6)$$

similar analysis shows that

$$|Y_1|_{\max}^2 = (A_{21}B_{12}C_{22} + A_{11}B_{11}C_{11})^2 \cdot |X_1|^2 \quad (3.7)$$

$$|Y_2|_{\min}^2 = \left[(A_{21}B_{22}C_{22})^2 + (A_{11}B_{21}C_{11})^2 + 2A_{11}A_{21}B_{21}B_{22}C_{11}C_{22} \cdot \cos(\beta_{21} - \beta_{22} + \beta_{12} - \beta_{11}) \right] \cdot |X_1|^2 \quad (3.8)$$

Hence, by adjusting the DC voltage applied to the PZT, the power out of outputs Y_1 and Y_2 can be varied. Subtracting Equations 3.5 and 3.8 and rearranging yields

$$\cos(\beta_{21} - \beta_{22} + \beta_{12} - \beta_{11}) = \frac{|Y_2|_{\max}^2 - |Y_2|_{\min}^2}{-4A_{11}A_{21}B_{21}B_{22}C_{11}C_{22} \cdot |X_1|^2} \quad (3.9)$$

From Figure 3.1 and Equations 2.11 and 2.12, it is apparent that the values of the terms $(A_{11}B_{21}C_{11})$ and $(A_{21}B_{22}C_{22})$ are obtained by disconnecting the appropriate input line to the second coupler and taking the square root of the ratio of the power from output Y_2 and the power into input X_1 . The maximum and minimum values for the power from output Y_2 are found by adjusting the PZT voltage. These values are used in Equation 3.9 to calculate the inherent phase shift of the coupler.

2. Response of PZT device

The fractional change in circumference of the PZT cylinder is given by the simplified tensor equation

$$\frac{\Delta C}{C} = d \cdot E + \chi \cdot \Delta T, \quad (3.10)$$

where ΔC is the change in the circumference, C is the circumference, E represents the electric field applied to the PZT between the inner and outer walls and ΔT is the change in temperature. The terms d and χ are proportionality constants relating the electric field and change in temperature, respectively, to the fractional change in the circumference. [Ref. 7]

The specific PZT used was the Channel Industries model 5800. This device has values of $d = 107 \times 10^{-12}$ (m/V), $\chi = 3.8 \times 10^{-6}$ (1/K) and $C = 37.7$ cm. The radial thickness of the PZT was 0.5 cm. Since the fiber was wrapped around the PZT twice before being secured in place with epoxy, the change in fiber length (ΔL) may be expressed as

$$\Delta L(\text{meters}) = 1.6 \cdot 10^{-8} \cdot V + 2.8 \cdot 10^{-6} \cdot \Delta T. \quad (3.11)$$

Assuming that the temperature is constant, an applied voltage of about 81 volts would result in a total optical path length change of 1300 nm, the wavelength of the laser source. From Equations 3.1, 3.2 and 3.11 we can see that by adjusting the voltage applied to the PZT, we can adjust the optical path difference and thus vary how the output power is shared between the two outputs. It is instructive to consider how reliably we can adjust the power between the outputs. If we consider the ideal coupler discussed in Section II.C, then Equations 3.1 and 3.2 simplify to

$$|Y_1|^2 = [0.5 - 0.5 \cdot \cos(\theta)] \cdot |X_1|^2 \quad (3.12)$$

$$|Y_2|^2 = [0.5 + 0.5 \cdot \cos(\theta)] \cdot |X_1|^2. \quad (3.13)$$

The lengths of the fibers used in the upper and lower legs of the system in Figure 3.1 are matched to a tolerance of 4 mm to minimize any effect of fiber temperature change. Therefore, the phase difference is related only to the change in circumference of the PZT. We can relate θ to the applied voltage by assuming that the PZT temperature remains constant and using Equation 3.11 to yield

$$\theta = 2\pi \frac{1.6 \cdot 10^{-8}}{1300 \text{ m}} = 2\pi \frac{V}{81}, \quad (3.14)$$

where V is the applied voltage in volts. This expression for θ is substituted into Equations 3.12 and 3.13 to yield

$$|Y_1|^2 = \left[0.5 - 0.5 \cdot \cos\left(2\pi \frac{V}{81}\right) \right] \cdot |X_1|^2 \quad (3.15)$$

$$|Y_2|^2 = \left[0.5 + 0.5 \cdot \cos\left(2\pi \frac{V}{81}\right) \right] \cdot |X_1|^2. \quad (3.16)$$

The expressions for the predicted normalized output powers are plotted as a function of applied voltage, along with measured data, in Figure 3.2 below. As shown

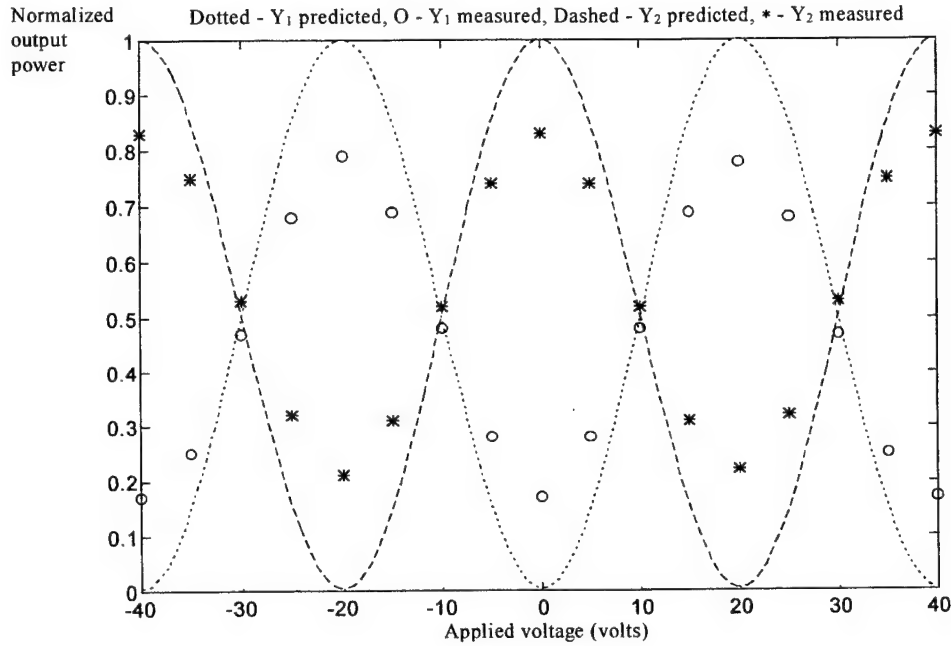


Figure 3.2. Response of Output Powers to PZT Applied Voltage

in Figure 3.2, the measured responses follow the predicted curves reasonably well.

However, the measured powers did not display the full predicted dynamic range. Since the operating wavelength of 1300 nm is above the cutoff wavelength of 1136 nm for the 8 μ m mode field diameter fiber in the system, only one optical mode was present [Ref. 8]. This indicates that the coupler did not split the power equally between the outputs, therefore preventing complete destructive or constructive interference. The sum of the measured values being constant shows that conservation of energy is obeyed by the coupler. This power-sharing pattern repeated as the PZT voltage was raised in steps of

approximately 40 volts. The power sharing worked with reverse bias applied to the PZT, which tends to compress the PZT, because the fiber was in tension when it was attached to the PZT.

3. Experimental Results

In order to determine the inherent phase shift of the coupler, the quantities needed in Equation 3.9 were measured and are given in Table 3.1.

$A_{11}B_{21}C_{11}$	$A_{21}B_{22}C_{22}$	$ Y_1 ^2_{max} / X_1 ^2$	$ Y_1 ^2_{min} / X_1 ^2$
0.403	0.342	0.564	0.115

Table 3.1. Measured Values for Phase Determination

Using the values in Table 3.1, the inherent phase shift of the coupler was calculated using Equation 3.9. The result, using this first method, is $145^\circ \pm 5^\circ$. The power fluctuations were such that the ratios in Table 3.1 are accurate to within 0.005, resulting in the $\pm 5^\circ$ uncertainty.

C. CALCULATION OF INHERENT PHASE SHIFT BY MEANS OF COUPLER EXCESS LOSS MEASUREMENT

1. Derivation

The second method of measuring the coupler phase shift uses a completely different approach. The development is similar to that used by Greene [Ref. 5] to show that the inherent phase shift for a lossless coupler must be 180° . By adding a term for the coupler loss into the derivation, a relationship between the coupler loss and the inherent phase shift can be found. Figure 3.3 shows a simple representation of a real 2x2 coupler. In Figure 3.3, X represents the electric field strengths at the inputs, Y represents the

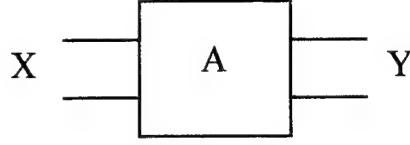


Figure 3.3. Simplified Representation of a 2x2 Coupler

electric field strengths at the outputs and A is the scattering matrix of the coupler.

Assuming that all fibers have the same cross section and attenuation, the sum of the output intensities, I_o , is the sum of the input intensities, I_i , minus the intensity lost in the coupler, I_L ,

$$I_o = I_i - I_L. \quad (3.17)$$

The intensities are proportional to the product of the respective electric field and its complex conjugate. Thus,

$$I_o = Y_1^* \cdot Y_1 + Y_2^* \cdot Y_2 = \bar{Y}^+ \cdot \bar{Y} \quad (3.18)$$

$$I_i = X_1^* \cdot X_1 + X_2^* \cdot X_2 = \bar{X}^+ \cdot \bar{X} \quad (3.19)$$

where the superscript $+$ represents the matrix adjoint, which is the complex conjugate of the transpose matrix. Since

$$\bar{Y} = \bar{A} \cdot \bar{X}, \quad (3.20)$$

substitution of Equations 3.18 through 3.20 into 3.17 yields

$$\bar{Y}^+ \cdot \bar{Y} = (\bar{A}\bar{X})^+ (\bar{A}\bar{X}) = \bar{X}^+ \bar{A}^+ \bar{A} \bar{X} = I_o = I_i - I_L = \bar{X}^+ \bar{X} - I_L = \bar{X}^+ \bar{I} \bar{X} - I_L, \quad (3.21)$$

where \bar{I} is a 2 by 2 identity matrix. Thus,

$$\bar{A}^+ \bar{A} = \begin{bmatrix} 1-L & 0-L \\ 0-L & 1-L \end{bmatrix}, \quad (3.22)$$

where L is the normalized intensity loss obtained by dividing I_L by I_i . The scattering matrix, A , can be represented by a 2x2 matrix of the form shown in Equation 2.4.

For a physically realizable system, the reciprocity theorem applied to the solution of Maxwell's equations in the coupler require [Ref. 5]

$$\tilde{A}_{mn} = \tilde{A}_{nm} \Rightarrow \alpha_{12} = \alpha_{21}. \quad (3.23)$$

Inserting Equations 2.4 and 3.23 into 3.22 and expanding yields

$$|A_{11}|^2 + |A_{12}|^2 = 1 - L \quad (3.24)$$

$$|A_{22}|^2 + |A_{21}|^2 = 1 - L \quad (3.25)$$

$$|A_{11}| \cdot |A_{12}| \cdot e^{j(\alpha_{12} - \alpha_{11})} + |A_{12}| \cdot |A_{22}| \cdot e^{j(\alpha_{22} - \alpha_{12})} = -L. \quad (3.26)$$

Taking the real and imaginary parts of Equation 3.26 yields

$$|A_{11}| \cdot |A_{12}| \cdot \cos(\alpha_{12} - \alpha_{11}) + |A_{12}| \cdot |A_{22}| \cdot \cos(\alpha_{22} - \alpha_{12}) + L = 0 \quad (3.27)$$

$$|A_{11}| \cdot |A_{12}| \cdot \sin(\alpha_{12} - \alpha_{11}) + |A_{12}| \cdot |A_{22}| \cdot \sin(\alpha_{22} - \alpha_{12}) = 0. \quad (3.28)$$

Solving Equations 3.24, 3.25, 3.27 and 3.28 reveals that

$$\cos(\alpha_{21} - \alpha_{22} + \alpha_{12} - \alpha_{11}) = \frac{L^2}{2|A_{11}|^2 \cdot |A_{12}|^2} - 1. \quad (3.29)$$

Thus, the second method of determining the inherent phase shift of a 2x2 coupler involves measuring the normalized power loss and the ratios of the output power from output one to the power into inputs one and two. From Equation 3.29 it is evident that for a lossless coupler, with $L = 0$, the ideal phase shift would be 180° . With any non-zero loss the phase shift will be something less than 180° .

2. Experimental Results

The quantities $|A_{11}|^2$ and $|A_{12}|^2$ are obtained by measuring the ratio of the output power from output one to the input power into inputs one and two, respectively, with the other input disconnected. The normalized power loss of the coupler, using a given input, is determined by subtracting the measured values for the two output powers from the input power and dividing by the input power. Using an input power of 459 μW into input one, the output powers measured for outputs one and two were 130 μW and 244 μW , respectively. Thus $|A_{11}|^2 = 0.28$, and the normalized coupler loss using input one, L_1 , is given by $L_1 = (459 - 130 - 244) / 459 = 0.185$. Putting the same input power into input two yields output powers of 177 μW and 202 μW . Thus the normalized coupler loss using input two, L_2 , is given by $L_2 = (459 - 177 - 202) / 459 = 0.174$ and $|A_{12}|^2 = 0.39$. The loss term, L^2 , is the product of the normalized power losses of the coupler when the input signal is coupled into ports one and two, so $L^2 = (0.174)(0.185)$. Using these values in Equation 3.29 yields a value of the coupler phase shift equal to $149^\circ \pm 6^\circ$, where the power measurement uncertainty of 4 μW caused the uncertainty of $\pm 6^\circ$.

D. APPLICATION OF AC VOLTAGE TO PZT TO DETERMINE PHASE SHIFT

1. Derivation

The third method used to measure the inherent phase shift of the 2x2 coupler was that devised by Schleip and Hereth [Ref. 2]. In this method, the identical setup was used as in the first method except that an AC voltage is applied to the PZT, as shown in Figure 3.4 below. With an AC voltage applied to the PZT, the circumference of the PZT and,

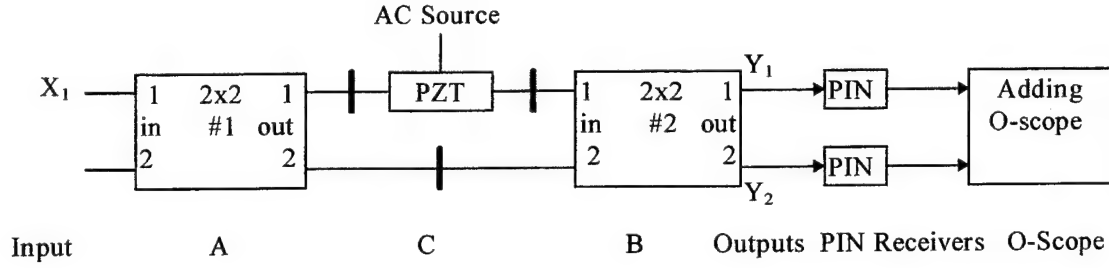


Figure 3.4. AC Modulated Phase Measurement

therefore, the optical path length of the fiber attached to it varies in a sinusoidal manner. Driving the PZT with an AC source may induce temperature fluctuations and therefore alter the length of the fiber attached to it. Since the PZT temperature was not controlled in this experiment, this effect may have caused some error. However, since the results are consistent with the other methods, this error is probably negligible. Thus, the difference in optical path, θ , is given by

$$\theta = \phi(t) + \Delta\theta, \quad (3.30)$$

where $\Delta\theta$ represents the steady-state difference in optical path due to the difference in physical length of the fibers and $\phi(t)$ represents the difference in optical path due to the length of the fiber attached to the PZT cylinder changing as a function of time due to the applied AC signal. Substituting Equation 3.30 for θ into Equations 3.1 and 3.2, the general expressions for $|Y_1|^2$ and $|Y_2|^2$, gives

$$|Y_1|^2 = \left[(A_{21}B_{12}C_{22})^2 + (A_{11}B_{11}C_{11})^2 + 2A_{11}A_{21}B_{11}B_{12}C_{11}C_{22} \cdot \cos(\phi(t) + \Delta\theta - \beta_{11} + \beta_{12} + \alpha_{21} - \alpha_{11}) \right] \cdot |X_1|^2 \quad (3.31)$$

$$|Y_2|^2 = \left[(A_{21}B_{22}C_{22})^2 + (A_{11}B_{21}C_{11})^2 + 2A_{11}A_{21}B_{21}B_{22}C_{11}C_{22} \cdot \cos(\phi(t) + \Delta\theta - \beta_{21} + \beta_{22} + \alpha_{21} - \alpha_{11}) \right] \cdot |X_1|^2. \quad (3.32)$$

The power in the output signals Y_1 and Y_2 has a time-invariant part, given by the first two terms, and a time-varying part given by the cosine terms in Equations 3.31 and 3.32.

Therefore, we can rewrite Equations 3.31 and 3.32 as

$$|Y_1|^2 = P_{Y1} + 2A_{11}A_{21}B_1B_2C_{11}C_{22}|X_1|^2 \cdot \cos(\phi(t) + \Delta\theta - \beta_{11} + \beta_{12} + \alpha_{21} - \alpha_{11}) \quad (3.33)$$

$$|Y_2|^2 = P_{Y2} + 2A_{11}A_{21}B_2B_2C_{11}C_{22}|X_1|^2 \cdot \cos(\phi(t) + \Delta\theta - \beta_{21} + \beta_{22} + \alpha_{21} - \alpha_{11}), \quad (3.34)$$

where P_{Y1} and P_{Y2} represent the time invariant power components. To simplify notation, let

$$\psi_1 = \Delta\theta - \beta_{11} + \beta_{12} + \alpha_{21} - \alpha_{11} \quad (3.35)$$

$$\psi_2 = \Delta\theta - \beta_{21} + \beta_{22} + \alpha_{21} - \alpha_{11} \quad (3.36)$$

$$p_{Y1} = 2A_{11}A_{21}B_1B_2C_{11}C_{22}|X_1|^2 \quad (3.37)$$

$$p_{Y2} = 2A_{11}A_{21}B_2B_2C_{11}C_{22}|X_1|^2. \quad (3.38)$$

Here p_{Y1} and p_{Y2} represent the amplitude of the time-varying portion of the output power and ψ_1 and ψ_2 represent the constant portion of the phase of these signals. Substituting Equations 3.35 through 3.38 into Equations 3.33 and 3.34 yields

$$|Y_1|^2 = P_{Y1} + p_{Y1} \cdot \cos(\phi(t) + \psi_1) \quad (3.39)$$

$$|Y_2|^2 = P_{Y2} + p_{Y2} \cdot \cos(\phi(t) + \psi_2). \quad (3.40)$$

If the output powers are added, the result is a time-varying power $P_{Y1+Y2}(t)$ given by

$$P_{Y1+Y2}(t) = P_{Y1} + P_{Y2} + p_{Y1} \cdot \cos(\phi(t) + \psi_1) + p_{Y2} \cdot \cos(\phi(t) + \psi_2). \quad (3.41)$$

The expression for P_{Y1+Y2} may be reduced to the form

$$P_{Y1+Y2}(t) = P_{Y1+Y2} + p_{Y1+Y2} \cdot \cos(\phi(t) + \psi_{1+2}), \quad (3.42)$$

where P_{Y1+Y2} is the time-invariant component. Algebraic manipulation leads to

$$(p_{Y1+Y2})^2 = (p_{Y1})^2 + (p_{Y2})^2 + 2p_{Y1}p_{Y2} \cdot \cos(\psi_1 - \psi_2) . \quad (3.43)$$

Solving for $\cos(\psi_1 - \psi_2)$ and substituting Equations 3.35 and 3.36 into Equation 3.43 yields

$$\cos(\beta_{12} - \beta_{11} + \beta_{21} - \beta_{22}) = \frac{(p_{Y1+Y2})^2 - (p_{Y1})^2 - (p_{Y2})^2}{2p_{Y1}p_{Y2}} . \quad (3.44)$$

Equation 3.44 gives an equation for the inherent phase shift of the coupler in terms of the time-varying output powers, p_{Y1} and p_{Y2} , and the time-varying sum of the output powers, p_{Y1+Y2} . This sum may be measured by calibrated detectors driving a dual-channel oscilloscope which has the capability of performing real-time addition of the two input signals.

2. Experimental Results

The system was configured as shown in Figure 3.4. The frequency at which the AC source was operated was 20 kHz and the applied voltage was 30 volts peak-to peak, although these values were not critical in measuring the phase shift. The outputs Y_1 and Y_2 were connected to PIN receivers. The outputs of the PIN receivers were summed in the oscilloscope. The length of the fibers from the outputs of the second coupler to the PIN receivers must be very closely matched so that the AC portion of the output powers can be properly added. The measured values needed to calculate the coupler inherent phase shift using Equation 3.44 are shown in Table 3.2. The units for the values in

p_{Y1}	p_{Y2}	p_{Y1+Y2}
6.4	8.0	4.4

Table 3.2. Measured Values for AC Modulation Method

Table 3.2 are simply divisions on the oscilloscope, each with an uncertainty of ± 0.2 .

Substituting these values into Equation 3.44 yields

$$\cos(\beta_{12} - \beta_{11} + \beta_{21} - \beta_{22}) = \frac{(4.4)^2 - (6.4)^2 - (8.0)^2}{2(6.4)(8.0)} = -0.835. \quad (3.45)$$

$$\beta_{12} - \beta_{11} + \beta_{21} - \beta_{22} = 147^\circ. \quad (3.46)$$

The value for the inherent phase shift of the coupler obtained using the AC modulation method was therefore $147^\circ \pm 3^\circ$.

E. CONCLUSION

In this chapter we investigated three distinct methods for measuring the inherent phase shift of a 2x2 coupler. The first method involved application of a DC voltage to the PZT in order to control the total path length of the fiber between output one of coupler one and input one of coupler two in Figure 3.1. Controlling the optical path difference between the upper and lower fibers allowed control of how the output power was shared between the two outputs. Figure 3.2 shows that adjusting this DC voltage resulted in the outputs sharing the power nearly as predicted. After measuring the quantities required in Equation 3.9, the calculated value of the inherent phase shift using this method was $145^\circ \pm 5^\circ$.

The second method involved measuring the excess loss of the coupler. Through the derivation in Section III.C, we showed that the normalized loss is related to the inherent phase shift by Equation 3.29. The calculated value of the inherent phase shift using this method was $149^\circ \pm 6^\circ$.

The third method, taken from Schliep and Hereth [Ref. 2], involved application of an AC voltage to the PZT as shown in Figure 3.4. This resulted in each of the output powers having quiescent and time-varying components. Using an adding oscilloscope, the quantities required by Equation 3.44 were measured to yield a calculated value of the inherent phase shift of $147^\circ \pm 3^\circ$.

Thus the three methods used all provided values of the inherent phase shift in the region of 147° . The ideal, lossless coupler has an inherent phase shift of 180° . The difference between the calculated values and the theoretical value is probably due to a combination of factors. One source of the potential error could be introduced by measuring the losses of the ST-ST connectors and attributing that to the excess loss of the coupler. The second factor is that the actual coupler measured is not lossless. The model coupler used has an advertised excess loss of less than 0.5 dB. If the coupler excess loss of 0.5 dB could be separated from the connector loss, a calculated value of the inherent phase shift could be found using the method derived in Section III.C. A coupler with balanced power sharing and excess loss of 0.5 dB would yield values of $L = 0.10$ and $|A_{11}|^2 = |A_{12}|^2 = 0.45$ giving an inherent phase shift of 167° . As shown in the next chapter, a realistic value for the excess coupler loss is about 0.1 dB. This corresponds to an inherent phase shift of 176° . Therefore the coupler excess loss accounts for between 4° and 13° of the difference between the ideal 180° inherent phase shift and the measured value. Since the measured values for the inherent phase shift were about 147° , the remaining difference is attributable to the loss associated with the ST connectors. Since

all the methods involve power measurements, any loss other than that of the coupler will make the measured phase shift appear further from the ideal value.

It is important to note that for the measured values of the inherent phase shift, the assumptions made in Section II.C for the system with ideal couplers are reasonably accurate. Therefore, the system outputs will nearly be approximated by Equations 2.29 and 2.30. This was shown experimentally by Heinbaugh [Ref. 1] during previous research conducted at the Naval Postgraduate School.

In the next chapter, we investigate methods to reduce the system loss found by Heinbaugh [Ref. 1] in previous experimental work.

IV. SYSTEM LOSS CONSIDERATIONS

A. PREVIOUS SYSTEM

1. System Design

The previous design, built and studied at the Naval Postgraduate School, is shown in Figure 4.1 below. The dark vertical lines represent ST-ST connections. The numerical values after 2x2 coupler #2 and at the outputs are the dB loss compared to the input power. In this design a third 2x2 coupler in the Y_2 output served as a 90 degree phase shifter. In order to balance the 3 dB loss inherent in the third coupler, a corresponding 3 dB attenuator was inserted in the fiber parallel to this stage in the Y_1 output. [Ref.1]

As explained in Chapter II, we have determined that the third coupler stage is unnecessary, and it is omitted in the two-stage design presented in this work. It was identified in previous work that the loss of this three-stage system was significant and that techniques for reducing its loss needed further investigation.

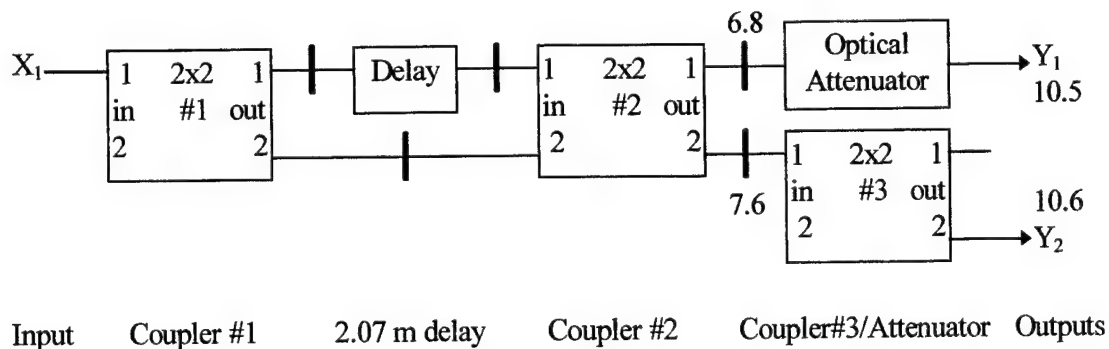


Figure 4.1. Previous System Design with dB Loss at Selected Points

2. System Loss

As reported by Heinbaugh [Ref. 1], the system experienced losses of 10.5 dB at output Y_1 and 10.6 dB at output Y_2 . The ideal system loss would be 6 dB at the outputs; 3 dB due to splitting the single input between the two outputs, plus 3 dB due to the attenuator and coupler #3. The difference between the ideal loss and that measured for this system was due to a combination of the excess coupler loss and the loss associated with the ST connectors. The couplers used in this system (Fiber Institute Sales Inc. model F193205) have advertised maximum excess loss of 0.5 dB. Therefore a maximum of 1.5 dB of the loss difference is due to the total coupler excess loss. Thus it can be assumed that the majority of the loss difference between the ideal and real system is due to the loss of the ST connectors and the ST-ST connections.

As shown in Figure 4.1, the measured loss after the second 2x2 coupler in the Y_1 channel was 6.8 dB and in the Y_2 channel was 7.6 dB. At this point in the system, the ideal loss would be 3 dB. Therefore, the large difference between the measured and ideal loss was due to the combination of excess loss from the two couplers and the loss associated with the ST connectors.

B. CURRENT DESIGN

The two-stage Mach-Zehnder Coupler is shown in Figure 4.2. The dark horizontal lines represent fusion splice connections between fibers. The numerical values at the outputs are the loss at the outputs. This system is the same as would result by terminating the previous design after the second 2x2 coupler and replacing the ST-ST connections by

fusion splices. It was shown in Chapter II that this design produces the desired “sum” and “difference” terms as shown by Equations 2.29 and 2.30. Heinbaugh showed that this system develops the predicted waveforms by supplying a 100 Mbps pseudo-random signal and measuring the signals at the outputs of the second coupler [Ref. 1]. This two-stage design was also shown to function in a multi-stage receiver in Section II.D. As shown in Figure 4.2, the measured system loss for the revised design is about 3.3 dB.

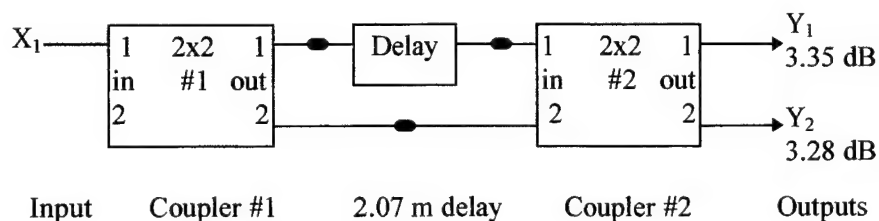


Figure 4.2. Current Design with dB Loss at Outputs

C. LOSS IMPROVEMENT ANALYSIS

1. Comparison of Previous and Current System Loss

Comparing Figures 4.1 and 4.2, it is apparent that the overall system loss has been reduced from approximately 10.5 dB to about 3.3 dB. This 7.2 dB improvement in performance is quite substantial. The previous design has an ideal system loss of 6 dB, whereas the two-stage design has an ideal loss of 3 dB, since the third coupler and corresponding attenuator are eliminated. Obviously, at least 3 dB of the improvement in system loss is simply due to recognizing that the two-stage system will perform the necessary function. If the system loss is compared at the outputs of the second coupler, the revised system displays between 3.5 dB and 4.3 dB improvement.

2. Analysis of Improvement

The revised system had a 3 dB overall advantage simply due to the exclusion of the third stage. However, the spliced two-stage system had an additional 3 dB to 4 dB improvement in loss performance at the output of the second coupler due to replacing the ST connectors and ST-ST connections with fusion splices. The ST connectors on the 2x2 couplers were installed by the manufacturer and have about 0.2 dB loss each. The ST-ST connections are plastic push-and-twist connections which align the single mode ST connectors. While taking power measurements in the laboratory, it was discovered that these devices are extremely sensitive to alignment and motion of the ST connectors. After a power measurement was made, the connection could be taken apart then re-connected, and the measured power would change up to 5%. While a power measurement was in progress, if the ST connectors were flexed with even a slight force, the power measurement may change by 5%. Therefore, measurements with the system using these ST-ST connections was very tedious and repeatable measurements were difficult to obtain.

The spliced system displayed very little power fluctuation during power level measurements. Without the loss induced by the ST connectors and their interconnections, the system loss was much lower. Prior to conducting the fusion splices on the system, several trial splices were conducted using manufactured fiber connection cables. The losses of the fiber connection cables were measured, then the cables were cut. The ends were prepared and then spliced back together in accordance with the Sumitomo Splicer

Manual [Ref. 9]. Post-splice loss measurements indicated that a reasonable estimate for the maximum loss per splice using the Sumitomo Fusion Splicer model 11X would be 0.2 dB for single mode fiber. Careful preparation of the fiber ends and exact alignment of the fibers prior to splicing were the critical factors in obtaining a low loss fusion splice. The system loss as shown in Figure 4.2 is very close to the ideal system loss of 3 dB. The measured loss values of 3.28 dB and 3.35 dB show that the actual coupler excess loss and total splice loss were quite small. Since the sum of the excess coupler loss and the total splice loss was about 0.3 dB, a reasonable estimate for the coupler excess loss would be about 0.1 dB.

In the system using ST connectors, a reasonable estimate for the total loss due to the ST connectors would be about 1.2 dB, since there are six ST connectors in the system, each having about 0.2 dB up to the output of the second coupler. Therefore about 3.0 dB of the loss measured at the output from the second coupler was due to the three ST-ST connections. As explained by Powers [Ref. 8], single mode connections are sensitive to angular misalignment and extremely sensitive to lateral misalignment. For example, an angular misalignment of 0.3 degrees or a 1 μm lateral misalignment would result in a 0.15 dB loss for the single mode fiber used with these 2x2 couplers. The manufacturer did not supply misalignment data for the ST-ST connection devices, but did supply a nominal 0.5 dB loss per ST-ST connection. Because of the way the actual measured power behaved during slight agitation of the ST-ST connector, this nominal value may only be accurate if the connection is made precisely and is then mechanically isolated. Clearly, replacing the

ST-ST connections with fusion splices substantially lowered the system loss and provided more stable operation.

3. Multi-stage Receiver

The loss of the previous three stage design using ST connectors was high enough that a multi-stage receiver may have poor performance. However, with a loss per stage on the order of 3.3 dB, a multi-stage receiver would have much better performance. For example, the receiver shown in Figure 2.2 would have about 21 dB total loss if the previous three stage design for the MZC were used. However, with the spliced two-stage MZC the receiver would have only about 6.6 dB loss.

In the next chapter, we will summarize the conclusions with regard to the MZC design, determination of the inherent phase shift of a 2x2 coupler, and the efforts undertaken to reduce the system loss.

V. CONCLUSIONS

We have considered an improved version of the Mach-Zehnder Coupler in this study. The previous design built and studied at the Naval Postgraduate School, shown in Figure 5.1, used three 2x2 single mode couplers with the fibers terminated using ST connectors. The third 2x2 coupler in the Y_2 output served as a 90 degree phase shifter. In order to balance the 3 dB loss inherent in the third coupler, a corresponding 3-dB attenuator was inserted in the fiber parallel to this stage in the Y_1 output [Ref.1].

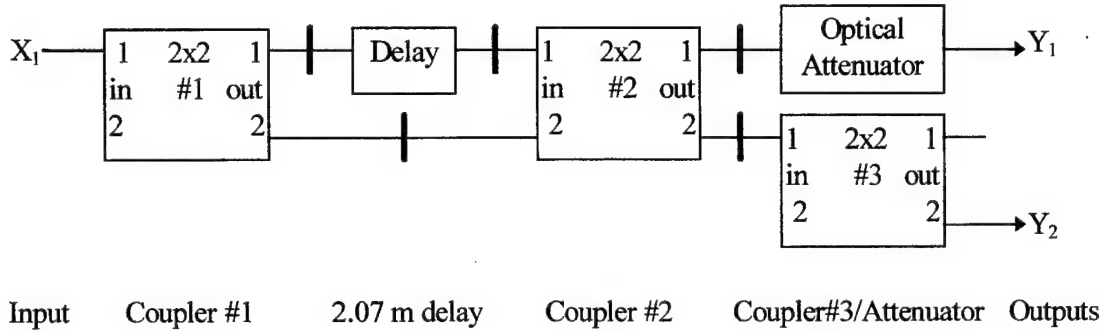


Figure 5.1. Previous Three-stage Design

As developed in Chapter II and shown experimentally in Heinbaugh's work [Ref. 1], the signals at the outputs of the second coupler contain the desired functions of the input signal given by Equations 2.31 and 2.32. Upon further analysis, we concluded that the third coupler stage is unnecessary and it is omitted in the two-stage design shown in Figure 5.2. In Chapter II we derived the exact expressions for the output signals for the two-stage design. We found that the required tolerance for the length of the delay fiber was equivalent to a small fraction of the data waveform bit period as opposed to a fraction

of the optical carrier wavelength. We have also shown in Section II.D that this two-stage design will function in a multi-stage receiver.

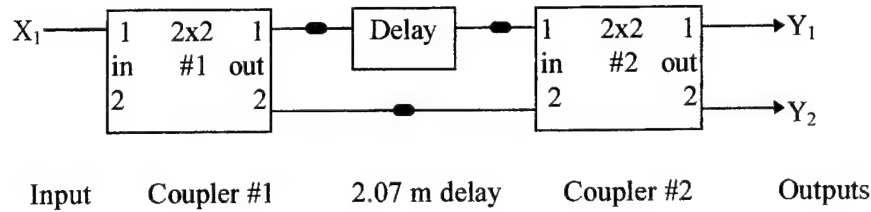


Figure 5.2. Two-stage Mach-Zehnder Coupler

Because the system uses the inherent phase shift of the 2x2 coupler to generate the sum and difference terms for the two outputs, one of the major goals of this work was to find a method whereby the inherent phase shift of a 2x2 coupler could be measured. We were able to derive and implement two separate techniques and use a third technique devised by Hereth and Schliep [Ref. 2] to verify our results.

The first method involved substituting a section of fiber wrapped around a PZT cylinder with a DC voltage applied for the delay line in Figure 5.2 in order to control the total path length of the fiber between output one of coupler one and input one of coupler two. A constant power laser operating at 1300 nm was applied to the first coupler at input X_1 . Controlling the optical path difference between the upper and lower fibers allowed fine control of how the output power was shared between the two outputs. Figure 3.2 shows that adjusting the DC voltage applied to the PZT resulted in the outputs sharing the power nearly as predicted. The development of this first method is given in Section III.B. After measuring the required quantities, the calculated value of the inherent phase shift was found using Equation 3.9 to be $145^\circ \pm 5^\circ$.

The second method involved measuring the excess loss of the coupler. Greene showed that the inherent phase shift of a lossless coupler would be 180° [Ref. 5]. Using a similar development, but including terms for loss, the derivation in Section III.C shows that the normalized loss is related to the inherent phase shift by Equation 3.29. The calculated value of the inherent phase shift using this method was $149^\circ \pm 6^\circ$.

The third method, taken from Schliep and Hereth [Ref. 2], involved application of an AC voltage to the PZT as shown in Figure 3.4. This resulted in each of the output powers having quiescent and time-varying components. Using an adding oscilloscope the quantities required by Equation 3.44 were measured to yield a calculated value of the inherent phase shift of $147^\circ \pm 3^\circ$.

The two methods we developed provided values of the inherent phase shift very close to that obtained using the third method. The difference between the calculated values and the theoretical value of 180° for a lossless coupler is due to a combination of factors. Since these methods all derive the coupler phase shift via power measurements, any loss other than the excess loss of the coupler will have the effect of making the calculated value of the phase shift further from the ideal value of 180° . The value of 147° is a worst-case estimate for the coupler phase shift, since much of the power loss occurred in the ST-ST connections. However, for the measured values of the inherent phase shift, the assumptions made in Section II.C for the system with ideal couplers are reasonably accurate. Therefore, the system outputs can be approximated by Equations 2.31 and 2.32. This was shown experimentally by Heinbaugh [Ref. 1] during previous research.

The other major focus of this work was on reducing the system loss. The measured loss of the previous system shown in Figure 5.1 was 10.5 dB [Ref. 1], while the ideal system loss would have been 6 dB. The measured loss after the second 2x2 coupler in the Y_1 channel was 6.8 dB and in the Y_2 channel was 7.6 dB. At this point in the system, the ideal loss would be 3 dB. This substantial overall loss and excess loss made it necessary to investigate design and construction modifications which would yield a more reasonable loss per stage.

Using the spliced two-coupler system, the overall system loss has been reduced to about 3.3 dB. This 7.2 dB improvement in performance is quite substantial. Obviously, 3 dB of the improvement is simply due to recognizing that the two-stage system will perform the necessary function. Additionally, the revised system displays between 3.5 dB and 4.3 dB improvement due to replacing the ST connectors and ST-ST connections with fusion splices. The loss of the previous three-stage design using ST connectors was high enough that a multi-stage receiver may have poor performance. However, with a loss per stage on the order of 3.3 dB, a multi-stage receiver would have much better performance.

The major goals of this work were met. Three separate methods for measuring the coupler inherent phase shift were conducted and yielded consistent results. The value of the inherent phase shift is such that the desired outputs are generated. The system loss has been reduced from 10.5 dB to 3.3 dB using design and construction modification. The two-coupler design will function in a multi-stage receiver.

Possible follow-on work would be to construct and test a complete receiver using the spliced two-stage Mach-Zehnder coupler as the building block.

LIST OF REFERENCES

1. Maryanne Heinbaugh, "The Mach-Zehnder Coupler," Master's Thesis, Naval Postgraduate School, Monterey, California, 1996.
2. F. Schliep and R. Hereth, "Phase Sensistive Measurement Technique for Singlemode Fibre Directional Couplers," *Electronics Letters*, Vol. 28, No. 16, pp. 1538-1540, July 1992.
3. Eugene Hecht, *Optics*, 3rd edition, pp. 403-404, Addison Wesley Longman, Inc., Menlo Park, California, 1997.
4. W. H. Steel, *Interferometry*, 2nd edition, pp. 123-124, Cambridge University Press, Cambridge, England, 1983.
5. Paul E. Greene, Jr., *Fiber Optic Networks*, pp. 70-79, 123-129, Prentice Hall, Englewood Cliffs, New Jersey, 1993.
6. K. G. Beauchamp, *Applications of Walsh and Related Functions*, Academic Press, Inc., Orlando, Florida, 1984.
7. Channel Industries, "Piezoelectric Ceramics," Channel Industries, Inc., Santa Barbara, California, 1984.
8. John Powers, *An Introduction to Fiber Optic Systems*, 2nd edition, Richard D. Irwin, Inc., Chicago, Illinois, 1997.
9. Sumitomo Electric Industries, "Instruction Manual for Optical Fiber Fusion Slicing Kit Type 11X," Sumitomo Electric, Ltd., Research Triangle Park, North Carolina, 1985.

INITIAL DISTRIBUTION LIST

1. Defense Technical Information Center 2
 8725 John J. Kingman Rd., STE 0944
 Ft. Belvoir, Virginia 22060-6218

2. Dudley Knox Library 2
 Naval Postgraduate School
 411 Dyer Rd.
 Monterey, California 93943-5101

3. Chairman, Code EC 1
 Department of Electrical and Computer Engineering
 Naval Postgraduate School
 Monterey, California 93943-5121

4. Professor John P. Powers, Code EC/Po 2
 Department of Electrical and Computer Engineering
 Naval Postgraduate School
 Monterey, California 93943-5121

5. Associate Professor D. Scott Davis, Code PH/Dv..... 2
 Department of Physics
 Naval Postgraduate School
 Monterey, California 93943-5117

6. Professor Tri T. Ha, Code EC/Ha 1
 Department of Electrical and Computer Engineering
 Naval Postgraduate School
 Monterey, California 93943-5121

7. LCDR Joseph S. Gildersleeve 1
 1013 Tuckerton Rd.
 Reading, Pennsylvania 19605